

Are Backscattering Ångström Exponents merely indicative of particles size? Advancing beyond by using light polarization

Alain Miffre and Patrick Rairoux

Université Claude Bernard Lyon 1, CNRS, Institut Lumière Matière, UMR 5306, F-69100, Villeurbanne, France
alain.miffre@univ-lyon1.fr

Abstract: Every day across the globe, dual-wavelength or multi-wavelength lidar instruments assess Backscattering Ångström Exponents (BAE_p), which delineate the wavelength-dependent behavior of particles backscattering coefficients. Traditionally regarded as a proxy for particle size in literature, we challenge this interpretation and propose a reevaluation leveraging light polarization. Specifically, by utilizing light polarization, we can independently extract the Backscattering Ångström Exponents of spherical (s) and non-spherical (ns) particles within a particle mixture (p) = $\{s, ns\}$, denoted as BAE_s and BAE_{ns} respectively. We establish and experimentally verify the relationship between BAE_p , BAE_s and BAE_{ns} , employing a case study involving mineral dust particles. Remarkably, BAE_s and BAE_{ns} can be simulated numerically using Mie theory for spherical particles and T-matrix numerical code for non-spherical particles, elucidating the influence of particle size and complex refractive index on these parameters. As a result, the range of involved (s) and (ns)-particles size or / and complex refractive index to be considered in lidar inversion algorithms, can be reduced, thus improving the accuracy of such retrievals. We believe this new methodology, published in [1], may then interest the lidar community: to be applied, it indeed only requires a $2\beta + 2\delta$ or multi-wavelength polarization lidar instruments, which are operated every day, worldwide.

1. Introduction

Multi-wavelength lidar instruments remotely evaluate particles Backscattering Ångström Exponent (BAE_p) is remotely evaluated every day from atmospheric [2–3] and is considered as a qualitative particle size indicator. Basically, BAE_p describes the wavelength dependence of the particles backscattering coefficient β_p between wavelength λ_1 and wavelength $\lambda_2 > \lambda_1$ [2]:

$$BAE_p = -\ln(\beta_{p,2}/\beta_{p,1})/\Lambda \quad (1)$$

where $\beta_{p,1} = \beta_p(\lambda_1)$, $\beta_{p,2} = \beta_p(\lambda_2)$ and $\Lambda = \ln(\lambda_2/\lambda_1) > 0$. As for β_p , BAE_p depends on the particle's size, shape and complex refractive index but difficult to disentangle. This is especially true after long-range transport, where particles presenting different sizes, shapes and refractive indices coexist. We here investigate the lidar backscattering Ångström exponent beyond the traditional interpretation of a particles size indicator. Our methodology [1] only requires a dual-wavelength polarization lidar instrument and light scattering numerical simulations and rely on the use of light

polarization to partition a a particle mixture (p) = $\{s, ns\}$, involving spherical (s) and non-spherical (ns) particles. Our new methodology is presented in Section 2. Section 3 is dedicated to the numerical simulations of BAE_s and BAE_{ns} while an application case study is proposed in Section 4.

2. BAE polarization methodology

From Eq. (1), we note that BAE_p is intensive, in contrary to β_p . Hence, the backscattering Ångström exponent BAE_p of a particles mixture (p) = $\{s, ns\}$ a priori differs from BAE_s and BAE_{ns} , the s and ns -particles backscattering Ångström exponents. To establish the relationship between BAE_p , BAE_s and BAE_{ns} , our starting point is the partitioning of a particles mixture into its spherical and nonspherical components using light polarization, as extensively described in [4, 5]. We first introduce the ratio $X_{ns} = \beta_{ns}/\beta_p$ of ns to p -particles backscattering coefficients. X_{ns} relates to the depolarization ratio δ_p of the particles mixture and to that δ_{ns} of its ns -particles as follows [4,5]: $X_{ns} = \delta_p(1 + 1/\delta_{ns})$. We then consider the ratio

$\beta_{p,2}/\beta_{p,1}$ and replace $\beta_{p,2}$ with $\beta_{s,2} + \beta_{ns,2}$. to finally get:

$$e^{-\Delta BAE_p} = e^{-\Delta BAE_s} + X_{ns,1} \times (e^{-\Delta BAE_{ns}} - e^{-\Delta BAE_s}) \quad (2)$$

where $X_{ns,1}$ is the value of X_{ns} at wavelength λ_1 . Eq. (5) states that BAE_p equals BAE_s (resp. BAE_{ns}) only when $X_{ns,1} = 0$ (resp. 1). In the most general case, at a given altitude, BAE_p must be discerned from BAE_s and from BAE_{ns} : BAE_p is not dedicated to s or ns-particles but BAE_s and BAE_{ns} are. BAE_s (resp. BAE_{ns}) then represents an unequivocal optical signature of the size distribution (SD) and complex refractive index (CRI) of considered s-particles (resp. ns-particles), in contrary to BAE_p .

3. Numerical simulations

Figure 1 shows the computed variations of BAE_s and BAE_{ns} as a function of the particles effective radius, real part and imaginary part of the CRI, by considering a mono-modal lognormal SD for s and for ns-particles, with geometrical standard deviation $\sigma = 1.5$, leading to a bimodal SD for p-particles.

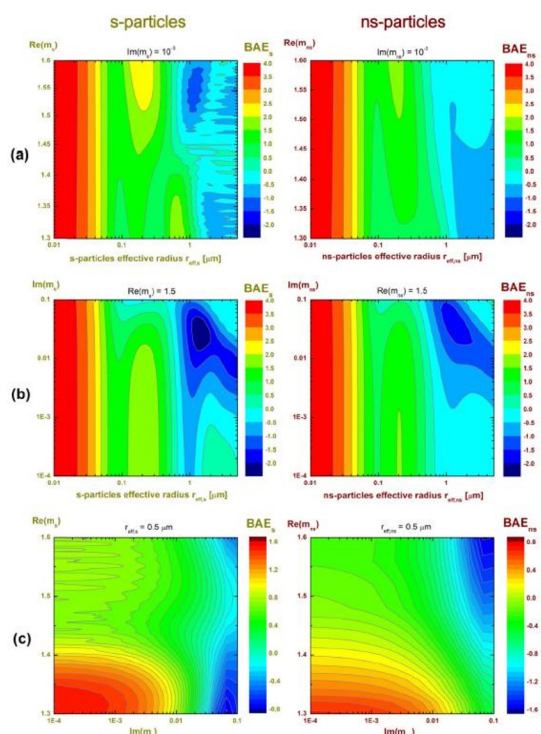


Figure 1. Contour plots at constant BAE_s (left) and BAE_{ns} (right) revealing the dependence of backscattering Ångström exponents with the SD (i.e., effective radius) and CRI (i.e., Re, Im).

For s-particles, Mie theory is applied, while for ns-particles, the MOPMAP code by Gasteiger and Wiegner [6], based on the T-matrix method and geometrical optics. Moreover, Figure 3 displays the variations of BAE_s (resp. BAE_{ns}) as a function of the effective radius $r_{eff,s}$ (resp. $r_{eff,ns}$) for) for sulfuric acid, ammonium sulfate and salt particles at RH = 0.8 (i.e. above their deliquescence point) for s-particles, then silica, aluminum oxide, iron oxide (hematite) and natural test dust, for ns-particles.

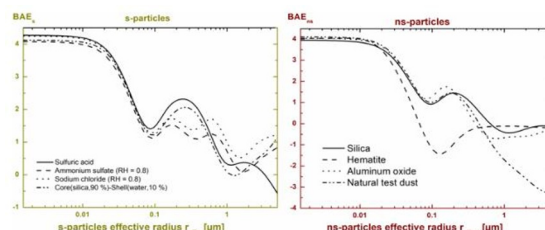


Figure 2. Computed variations of BAE_s (left) and BAE_{ns} (right) at ($\lambda_1 = 355$ nm, $\lambda_2 = 532$ nm) as a function of $r_{eff,s}$ and $r_{eff,ns}$ for concrete case studies.

4. Application case study

As an application case study, we examined a Saharan dust event that affected Lyon, France, as detailed in our publication [7]. Utilizing our unique $2\beta+2\delta$ polarization lidar instrument [4], any polarization and wavelength cross-talk were minimal, ensuring clear retrievals of vertical profiles for $(\beta_p, \beta_s, \beta_{ns})$. Subsequently, these profiles allowed for the derivation of corresponding Ångström exponents (BAE_p, BAE_s, BAE_{ns}), as depicted in Fig. 3, employing wavelengths $\lambda_1 = 355$ nm and $\lambda_2 = 532$ nm. At altitudes above 2.5 km, where the dust cloud is present, BAE_p consistently falls between BAE_s and BAE_{ns} , approaching BAE_s only when $X_{ns,1}$ is nearly zero. Through our in-depth analysis of the case study [7], we found that sulfuric acid particles predominantly constituted the s-particles, resulting from particle growth subsequent to a nucleation event triggered by mineral dust [7]. For the sake of our discussion, let's focus on the altitude of 2.7 km, where $BAE_s = 2.3 \pm 0.6$ and $BAE_{ns} = -0.8 \pm 0.1$. By utilizing the refractive indices of sulfuric acid and natural test dust, obtained from Fig. 2, we were able to deduce a range of effective radii for both s and ns-particles. Intriguingly, the retrieved range of effective radii accurately mirrors the underlying

microphysics: with $BAE_s = 2.7 \pm 0.5$ at 2.7 km altitude, the effective radius ($r_{eff,s}$) falls within the range of either 40 ± 10 nm or 250 ± 80 nm when considering sulfuric acid particles from Fig. 2, consistent with nucleation providing very small sulphuric acid particles in the vicinity of larger dust particles [7]. Meanwhile, for $BAE_{ns} = -1.4 \pm 0.8$, larger $r_{eff,ns}$ values are obtained, ranging from 1.1 ± 0.5 μ m when natural test dust ns-particles are considered from Fig. 1. In conclusion, our novel methodology enables the evaluation of the range of particle radii involved, faithfully capturing the underlying microphysics. It's worth noting that if BAE_p had been considered instead of BAE_s and BAE_{ns} , the retrieved effective radii range would have differed noticeably: $BAE_p = 1.4 \pm 0.3$ would have led to 550 ± 90 nm for $r_{eff,s}$ and 200 ± 50 nm for $r_{eff,ns}$.

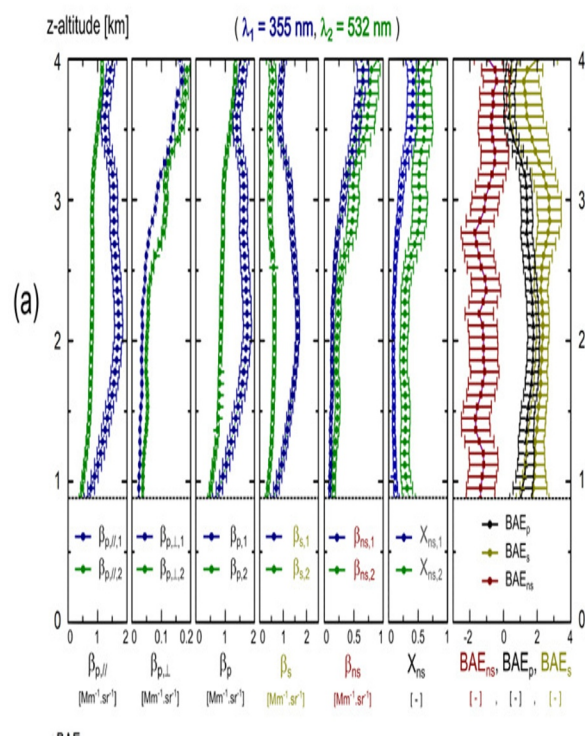


Fig. 3. Lidar profiles of particles backscattering ($\beta_p, \beta_s, \beta_{ns}$) at wavelength pair ($\lambda_1 = 355$ nm in blue, $\lambda_2 = 532$ nm in green) and corresponding Ångström exponents (BAE_p, BAE_s, BAE_{ns}) for p, s, ns-particles backscattering during a dust nucleation event at Lyon (France, July 2nd 2015, 14h UTC) taken as a case study. The difference in the (BAE_p, BAE_s, BAE_{ns}) profiles originates from $X_{ns,1}$ (or $X_{ns,2}$).

5. Conclusion and outlook

This contribution presents a novel approach for interpreting vertical profiles of backscattering Ångström exponents, moving beyond the conventional view of them solely as indicators of particle size, as detailed in our previous publication [1]. Specifically, our method employs a precise $2\beta + 2\delta$ polarization lidar instrument to extract vertical profiles of backscattering Ångström exponents (BAE_s and BAE_{ns}) tailored to spherical (s) and non-spherical (ns) particles. By numerically simulating BAE_s and BAE_{ns} , we can quantify their dependence on particle size and complex refractive index. Consequently, the specific vertical profiles of BAE_s and BAE_{ns} enable the identification of a range of effective radii or complex refractive indices involved, transcending the traditional interpretation of backscattering Ångström exponents solely as indicators of particle size. While our methodology offers absolute ranges for particle effective radii or refractive indices, obtaining more precise values necessitates solving the inverse problem, which exceeds the scope of this communication due to its complexity. Nonetheless, our approach can complement inversion algorithms to enhance retrieval accuracy by narrowing the search space, i.e., reducing the range of effective radii or complex refractive indices considered for both spherical and non-spherical particles.

6. References

- [1] Miffre, A., D. Cholleton, P. Rairoux: *On the use of light polarization to investigate the size, shape and refractive index of backscattering Angstrom exponents*, Opt. Lett. **45**(5), 1084–1087 (2020).
- [2] Haarig, M., A. Ansmann, H. Baars, C. Jimenez, I. Veselovskii, R. Engelmann, and D. Althausen: *Depolarization and lidar ratios at 355, 532, and 1064 nm and microphysical properties of aged tropospheric and stratospheric Canadian wildfire smoke*, Atmospheric Chem. Phys. **18**, 11847–11861 (2018).

- [3] Sugimoto, N., and C. H. Lee: *Characteristics of dust aerosols inferred from lidar depolarization measurements at two wavelengths*, *Appl. Opt.* **45**, 7468–7474 (2006).
- [4] Mehri, T., O. Kemppinen, G. David, H. Lindqvist, J. Tyynelä, T. Nousiainen, P. Rairoux, and A. Miffre, *Investigating the size, shape and surface roughness dependence of polarization lidars with light-scattering computations on real mineral dust particles: Application to dust particles' external mixtures and dust mass concentration retrievals*, *Atmos. Res.* **203**, 44–61 (2018).
- [5] David, G., B. Thomas, T. Nousiainen, A. Miffre, and P. Rairoux, *Retrieving volcanic, desert dust, and sea-salt particle properties from two/three-component particle mixtures after long-range transport using UV-VIS polarization Lidar and T-matrix*, *Atmos. Chem. Phys.* **13**, 6757–6776, (2013).
- [6] J. Gasteiger and M. Wiegner, [Geosci. Model Dev.](#) **11**, 2739 (2018).
- [7] Miffre, A., D. Cholleton, T. Mehri, P. Rairoux, *Remote Sensing Observation of New Particle Formation Events with a (UV, VIS) Polarization Lidar*, *Rem. Sens.* **11**, 1761 (2019).